ACS APPLIED BIO MATERIALS

www.acsabm.org Article

Label-Free Antifouling Photoelectrochemical Sensing Strategy for Detecting Breast Tumor Cells Based on Ligand–Receptor Interactions

Ning Gao,† Bobo Fan,† Li Li, Xiaojun Sun, Xueying Wang, Hongmin Ma,* Qin Wei,* and Huangxian Ju

Cite This: *ACS Appl. Bio Mater.* 2021, 4, 4479–4485 Read Online

ACCESS | Metrics & More | Article Recommendations | Supporting Information

ABSTRACT: Biomarker expression both on the cell surface and in serum is directly related to the pathological process of tumor. Based on the interaction between the ligand and the protein receptor, a label-free photoelectrochemical (PEC) biosensing interface with good antifouling ability was proposed for tumor cell detection. TiO_2 nanotube (NT) arrays were used as the substrate to enhance the ability of the biosensor to capture the target. Mercapto-terminated 8-arm poly(ethylene glycol) was introduced onto the electrode surface by the deposition of Au nanoparticles on TiO_2 NTs, creating an antifouling molecular layer. The recognition ligand hyaluronic acid (HA) was functionalized by dopamine and introduced onto the sensing surface based on the unique chelating interaction between the catechol group and the titanium atom. Benefitting from the specific recognition of HA with CD44 and the 3D porous structures of NTs, the constructed PEC biosensor showed excellent abilities toward the detection of MDA-MB-231 breast tumor cells and the soluble form of CD44. The ligand–receptor PEC sensing strategy has promising potential for the detection of tumor cells and protein biomarkers.

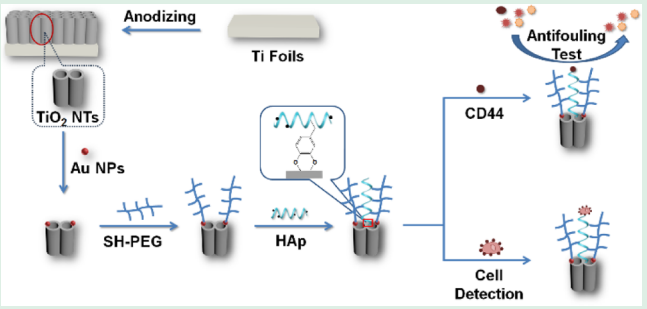

KEYWORDS: *antifouling, ligand receptor, tumor cells, photoelectrochemical biosensor, soluble CD44*

1. INTRODUCTION

CD44, a glycoprotein, is overexpressed on the surface of tumor cell membranes. Furthermore, CD44 is associated with the growth and metastasis of tumor cells, making it an important tumor marker.[1,2] The researchers found that CD44 can be specifically recognized by the polysaccharide ligand hyaluronic acid (HA), making it possible to diagnose and treat tumors.[3,4] HA is widely used in fluorescence imaging,[5] targeted drug delivery,[6,7] and enrichment of tumor cells[8] due to its higher stability, easier functionalization, and lower cost. However, the direct in vitro detection of tumor cells based on the recognition between ligands and biomarkers has rarely been reported.[9] More importantly, the concentration of tumor cells in the peripheral blood is closely related to the pathological process of patients, and the accurate detection of tumor cell concentration is of great significance for the clinical treatment of cancer patients.[10]

Photoelectrochemical (PEC) biosensors have received increasing attention due to their simple operation, low background signal, and good sensitivity.[11−14] As a traditional photoelectric semiconductor material, TiO_2 is often used to construct PEC biosensors due to its simple preparation, large specific surface area, especially stable chemical properties and large photocurrent density.[15] Hence, TiO_2 has been widely used in catalysis, solar cells, and other fields.[16−18] The interface constructed by three-dimensional (3D) nanomaterials and modified by specific biomolecules (e.g., ligand, antibody, and aptamer) has been shown to have surprising interactions with biomarkers and cells.[19,20] For example, functionalized TiO_2 nanotube (NT) arrays show a higher efficiency in capturing cells than two-dimensional (2D) planar substrates. However, the porous structure may lead to poor antifouling performance and selectivity of the biosensors constructed by TiO_2 NTs, and the compositions in peripheral blood are more complex. Therefore, it is necessary to construct an antifouling interface on the biosensor to reduce the influence of nonspecific adsorption of proteins and other nontarget substances. In the previous work, we introduced poly(ethylene glycol) (PEG) to improve the antifouling ability of a PEC biosensor.[21] The good hydrophilicity makes PEG exhibit amazing antifouling ability, which enables it to be widely used in drug delivery and antifouling interface construction.[22,23]

Received: February 17, 2021
Accepted: April 5, 2021
Published: April 15, 2021

https://doi.org/10.1021/acsabm.1c00215
ACS Appl. Bio Mater. 2021, 4, 4479–4485

Scheme 1. (A) Schematic Diagram of HAp Preparation; (B) Schematic Representation of the Construction Process of PEC Biosensors and the Recognition Abilities toward the Cell

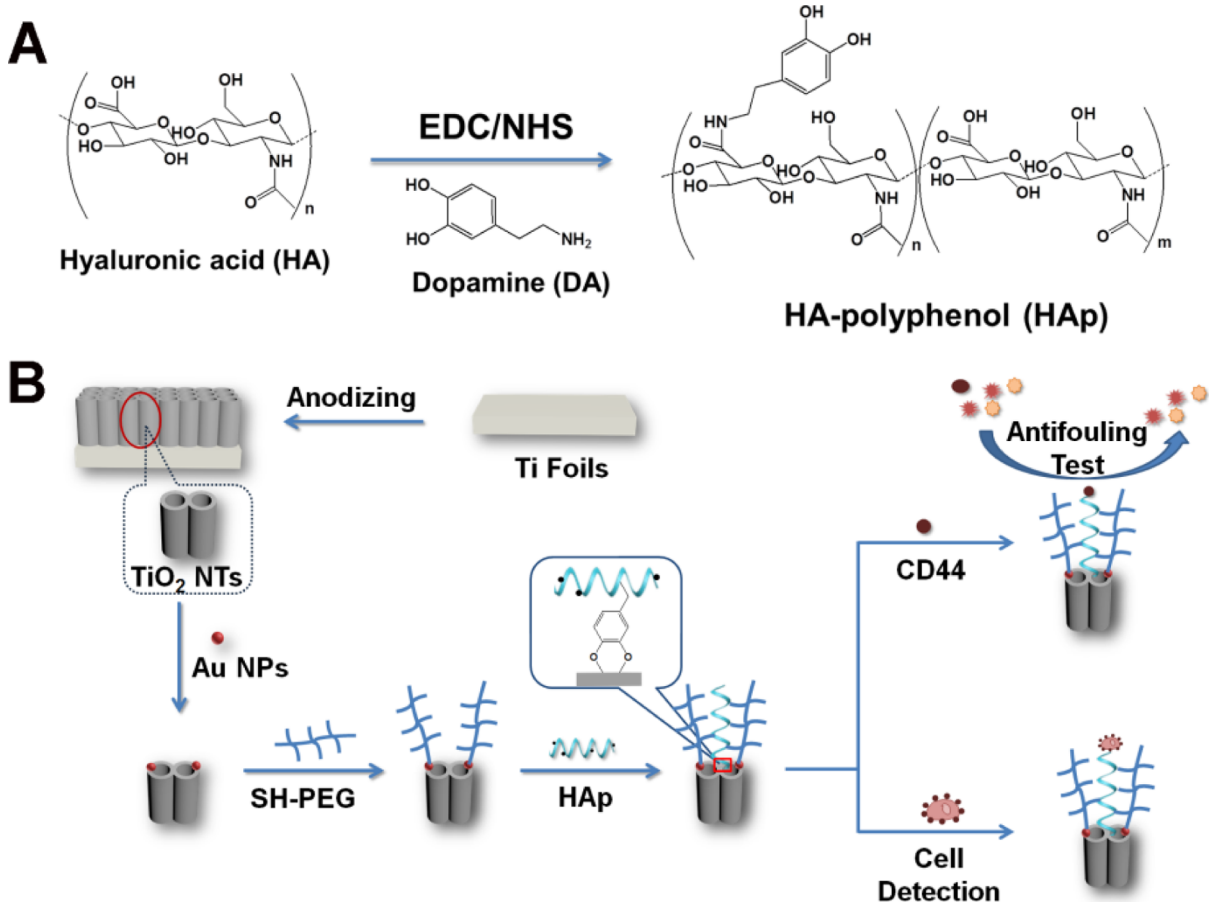

Dopamine (DA) with good biocompatibility and no toxicity is a neurotransmitter found in the central nervous system of mammals.[24] Deposition of noble metal nanoparticles (NPs) is often used for surface functionalization to provide binding sites for molecules.[25,26] DA has the amino and catechol structure, which allows it to form coordination bonds, covalent bonds, and hydrogen bonds with other materials.[27−29] In addition, DA can polymerize under alkaline conditions to form polydopamine which can stick to almost any interface. Therefore, DA is often used to modify materials and interfaces.[30,31]

In this work, TiO_2 NTs as a sensor substrate were obtained by anodizing Ti sheets. The Au NPs were then deposited on the TiO_2 NT surface by chronoamperometry. Through the interaction of Au and mercapto-terminated 8-arm poly(ethylene glycol) (SH-PEG), a self-assembled monolayer film is formed on the surface of Au NPs, taking advantage of the Au−sulfur bond, thereby modifying PEG onto the electrode. In order to modify HA onto the electrode, the functionalization of HA is achieved by the coupling reaction between the hydroxyl group of HA and the amino group of DA (Scheme 1A). DA coupled with HA to form HA-polyphenol (HAp) with a catechol structure. Due to the reaction between catechol and TiO_2 NTs, HAp formed a self-assembled monolayer film on the electrode surface. Finally, MDA-MB-231 cell ($CD44^+$) as a model cell was captured on the TiO_2 NTs/Au/PEG/HAp electrode surface based on the strong recognition ability between CD44 and HAp. A high-sensitivity PEC biosensing interface with outstanding antifouling ability and no cell damage was constructed to detect the MDA-MB-231 cell (Scheme 1B) and soluble CD44. This biosensor has excellent clinical application prospects and provides a new thought for the specific and sensitive detection of tumor cells and soluble CD44.

2. EXPERIMENTAL SECTION

2.1. Preparation of HAp. According to previously reported methods,[32−34] HAp was synthesized by the carbodiimide coupling reaction (Scheme 1A). At first, 250 mg HA was completely dissolved in 40 mL of degassed phosphate-buffered saline (PBS) (0.1 M, pH = 5.5). After this, 120 mg of 1-ethyl-3(3-dimethylaminopropyl) carbodiimide (EDC) and 72 mg of *N*-hydroxysuccinimide (NHS) were tardily added and magnetically stirred for 40 min. Subsequently, 142 mg of DA was added to the above solution and stirred for 20 h under the protection of argon. Then, the resulting product was dialyzed (7 kDa dialysis bag) by PBS for 72 h for purification. Finally, the solution was lyophilized to obtain a white product.

2.2. Preparation of TiO_2 NTs/Au NPs Electrodes. The detailed preparation process of the TiO_2 NTs electrodes is provided in the Supporting Information.

The TiO_2 NTs/Au electrode was prepared by electrodeposition. The TiO_2 NTs electrode was soaked in a $HAuCl_4$ solution (10 mL, 1 mM) for the cycle of electrodeposition. 60 electrodeposition cycles were performed, and each electrodeposition cycle lasted for 0.5 s at a constant potential of −3 V.

2.3. Cell Culture and Treatment. The medium was prepared by mixing 90 mL of Dulbecco's modified Eagle's medium supplemented with 10 mL of fetal bovine serum and 1 mL of dual antibody (penicillin−streptomycin) solution. MDA-MB-231 cells were cultured to logarithmic phase in culture bottles containing culture medium in a

https://doi.org/10.1021/acsabm.1c00215
ACS Appl. Bio Mater. 2021, 4, 4479−4485

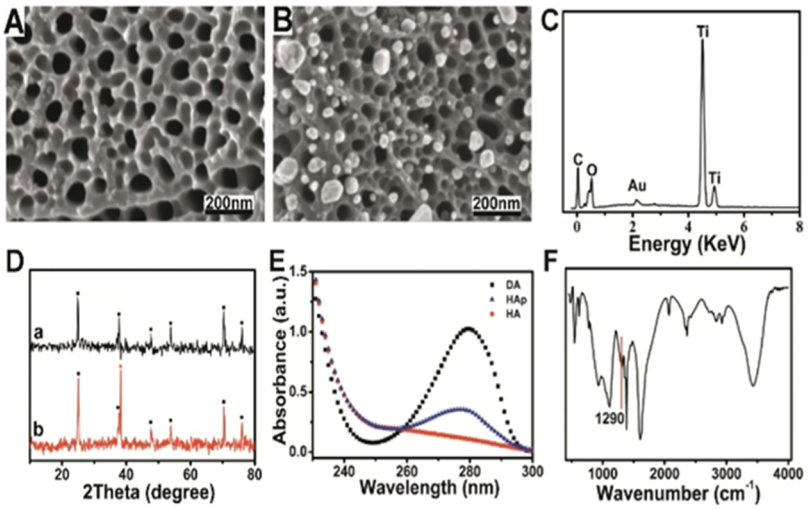

Figure 1. SEM image of TiO_2 NTs (A) and TiO_2 NTs/Au (B); EDS pattern (C) of TiO_2 NTs/Au; XRD pattern (D) of TiO_2 NTs (a) and TiO_2 NTs/Au (b); UV−vis absorbance spectra (E) of DA, HAp, and HA; and FT-IR spectra (F) of HAp.

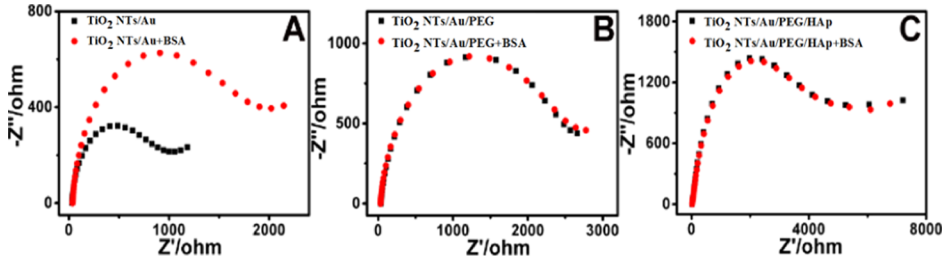

Figure 2. EIS Nyquist change diagrams of different modified electrodes after immersion in 500 ng/mL BSA solution: (A) TiO_2 NTs/Au; (B) TiO_2 NTs/Au/PEG; and (C) TiO_2 NTs/Au/PEG/HAp.

humid environment with a temperature of 37 °C and CO_2 concentration of 5.00%. The cells were then digested with 0.25% trypsin−ethylenediaminetetraacetate and centrifuged for 10 min at 1000 rpm. The obtained cell precipitate was dispersed in medical PBS (pH = 7.4) for use in the next step, and the concentration of the dispersed cell suspension was calculated with a hemocytometer.

2.4. Preparation of the PEC Biosensing Platform. As depicted in Scheme 1B, SH-PEG was modified onto TiO_2 NTs/Au electrodes by the action of Au and SH for 0.5 h. After washing, the TiO_2 NTs/Au/PEG electrodes were soaked in the freshly prepared HAp (2 mg/mL) in the Tris−HCl solution (0.1 M, pH = 8.5). Thus, HAp is fixed to the electrode for 0.5 h through the coordination reaction of Ti and the catechol structure in HAp. After washing with Tris−HCl solution to remove any unbound HAp, the TiO_2 NTs/Au/PEG/HAp electrode was obtained. Finally, the PEC biosensing interface was successfully built. All the soaking was performed at 4 °C.

2.5. PEC and EIS Detection of the Target. All tests in this experiment were performed with the traditional three-electrode system: the reference electrode was a saturated calomel electrode, a platinum wire electrode was used as the counter electrode, and the working electrode was a prepared composite electrode. PEC detection was conducted in PBS (pH = 7.4) containing 0.1 M AA. The photocurrent was obtained under a bias voltage of 0 V; the excitation light intensity was 180 $W{\cdot}m^{-2}$ with a wavelength of 450 nm to acquire the photocurrent. The EIS test was carried out in an electrolyte solution containing 2.5 mM $K_3Fe(CN)_6$ and 0.1 M KCl. The AC amplitude was 5 mV, and the frequency range was set to 10^{-1} Hz ~ 10^5 Hz, with no light.

2.6. Antifouling Property Test. EIS and PEC responses were used to evaluate the antifouling property of the prepared sensing platform. After soaking in 500 ng/mL BSA solution in PBS (0.1 M, pH = 7.4) for 0.5 h, the change of the same electrode was measured. In addition, Hb and IgG were used as interfering substances to carry out the same antipollution experiment test.

2.7. PEC Characterization. The conditions for the sensor preparation and sensing were selected (Figures S2 and S3).

The selectivity was investigated by comparing the photocurrent and EIS responses of the TiO_2 NTs/Au/PEG/HAp electrode soaked in the MDA-MB-231 cell (500 cell/mL) solution, the mixed solution of MDA-MB-231 cell (500 cell/mL) and BSA (500 ng/mL), and the mixed solution of MDA-MB-231 cell (500 cell/mL), BSA (500 ng/mL), Hb (500 ng/mL), and IgG (500 ng/mL), respectively. The photocurrent of the PEC biosensor modified with the MDA-MB-231 cell (500 cell/mL) within 580 s was recorded to detect the output signal stability. The photocurrent of the TiO_2 NTs/Au/PEG/HAp electrode was then measured after a week of storage at 4 °C to study the storage stability. The photocurrents of the five TiO_2 NTs/Au/PEG/HAp electrodes modified with the MDA-MB-231 cell (500 cell/mL) were compared to assess the reproducibility.

3. RESULTS AND DISCUSSION

3.1. Loading of Au NPs on the TiO_2 NTs and Characterization of HAp. By comparing the SEM images of TiO_2 NTs (Figure 1A) and TiO_2 NTs/Au (Figure 1B), it can be clearly seen that Au NPs were successfully deposited onto TiO_2 NTs. After the EDS characterization (Figure 1C) of the TiO_2 NTs/Au electrode, it was found that the main elements of the electrode were Ti, O, C, and Au, which proved that the TiO_2 NTs/Au electrode was successfully prepared. In addition, in the XRD analysis (Figure 1D), as shown in curve (a), the corresponding peaks (101), (004), (200), (105), (220), and (215) appeared at 25.29, 37.80, 48.05, 53.89, 70.31, and 75.03°, proving that the TiO_2 NTs were of anatase form

https://doi.org/10.1021/acsabm.1c00215
ACS Appl. Bio Mater. 2021, 4, 4479−4485

(JSPDS 21-1272). As shown in curve (b), in addition to the characteristic peak of TiO_2 NTs, the characteristic peak (111) of Au appeared at 38.18° (JSPDS 04-0784). The existence of C, O, Ti, and Au elements was shown in the full survey spectrum of XPS (Figure S11). The two peaks at 458.5 and 464.2 eV correspond to Ti $2p_{3/2}$ and Ti $2p_{1/2}$. It can be seen that the two peaks at 531.8 and 530.5 eV correspond to the binding energy of O 1s in TiO_2 NTs. It is worth noting that the two peaks at 86.6 and 84.2 eV can be distributed to the binding energies of Au $4f_{5/2}$ and Au $4f_{7/2}$. Therefore, the results indicated that the TiO_2 NTs/Au electrode was successfully prepared.

The prepared HAp was characterized by UV−vis absorbance (Figure 1E) and FT-IR (Figure 1F) spectroscopy. The catechol structure in DA had an absorption peak at 280 nm in the UV−vis absorbance spectra.[35] As shown in Figure 1E, the prepared HAp had an absorption peak at 280 nm, and HA had no absorption peak. This proved that DA was successfully modified onto HA. As shown in Figure 1F, the characteristic peak of the amide bond appeared at 1290 and 1670 cm^{-1}, which demonstrated that HAp was successfully obtained via modifying DA to HA by the carbodiimide coupling reaction (Scheme 1A).

3.2. Antifouling Performance of the PEC Biosensing Interface. As shown in Figure 2A, the R_{et} value of the TiO_2 NTs/Au electrode transformed to a significantly higher value after immersion in the BSA solution. This is because the Au NPs on the TiO_2 NTs/Au electrode provides binding sites for BSA, so that more amount of BSA is adsorbed on the TiO_2 NTs/Au electrode surface, which increases the R_{et} value. However, PEG has strong hydrophilicity and steric repulsion, thereby preventing BSA from polluting the TiO_2 NTs/Au/PEG electrode. As expected, the R_{et} value of the TiO_2 NTs/Au/PEG electrode was almost the same (Figure 2B). The effect of HAp on the antifouling property of the electrode was further investigated. It can be seen from Figure 2C that the R_{et} value of the TiO_2 NTs/Au/PEG/HAp electrode was basically unchanged before and after soaking in BSA solution, which proves that the TiO_2 NTs/Au/PEG/HAp electrode has outstanding antifouling function. The introduction of HAp does not affect the antifouling property of the electrode, which may be related to the hydrophilic capacity of HA. Similarly, the EIS test also demonstrated that the PEC biosensor showed excellent antifouling property toward IgG and Hb (Figure S4).

3.3. Photoelectric and Electrochemical Behavior of the Fabricated PEC Biosensor. The construction process can be monitored by the change of photocurrent responses (Figure 3A). It can be found that the photocurrent of the TiO_2 NT electrode [curve (a)] was about 93.5 μA, which was due to the good photoelectric properties of TiO_2. After modifying the surface of the TiO_2 NT electrode with Au NPs [curve (b)], the photocurrent was lowered. This may be because the Fermi level of TiO_2 is higher than that of Au, and some photogenerated electrons of TiO_2 NTs flow into Au NPs to balance the Fermi level.[36] UV−vis diffuse reflectance absorption spectra are shown in Figure S12. The TiO_2 NT electrode exhibited a photoresponse only in the UV region with a wavelength of less than 400 nm, which was caused by the inherent band gap of TiO_2.[37] After the deposition of Au NPs, the light absorption was significantly enhanced in the wavelength range of 400−800 nm, and the absorption edge was red-shifted. This was attributed to the low-energy transition between the TiO_2 valence band and the introduced local energy level.[38,39] Thereafter, the photocurrent decreased with the modifications of PEG [curve (c)] and HAP [curve (d)]. This was attributed to the fixation of PEG and HAp that blocked the surface reaction of AA and the photoinduced pores to a certain extent. When MDA-MB-231 was captured onto the surface of the TiO_2 NTs/Au/PEG/HAp electrode by the specific binding of CD44 and HAp [curve (e)], the photocurrent was further reduced.

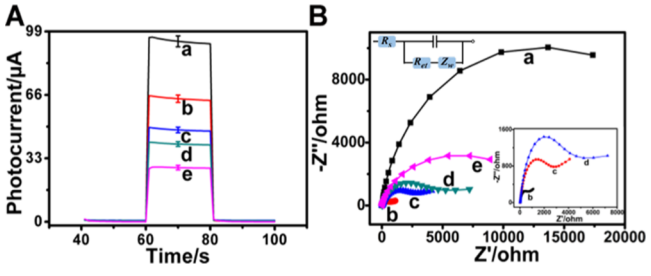

Figure 3. Photocurrent (A) and EIS (B) response curves of different decorated electrodes: (a) TiO_2 NTs; (b) TiO_2 NTs/Au; (c) TiO_2 NTs/Au/PEG; (d) TiO_2 NTs/Au/PEG/HAp; and (e) TiO_2 NTs/Au/PEG/HAp/cell.

EIS is also an effective means to characterize the surface modification of electrodes in the construction process (Figure 3B). The R_{et} value of the TiO_2 NT electrode [curve (a)] was larger, which was due to the characteristics of semiconductor materials. Due to the excellent conductivity of Au, the semicircular portion of the EIS curve of the TiO_2 NTs/Au electrode [curve (b)] was very small. With the decoration of PEG and HAp [curve (c,d)], the R_{et} values of the electrodes gradually increased. This may be due to the presence of PEG and HAp, as weakly conductive polymers can hinder electron transfer. When MDA-MB-231 was modified onto the TiO_2 NTs/Au/PEG/HAp electrode [curve (e)], the R_{et} value of the electrode was greatly increased due to the poor conductivity of the protein. The change in the R_{et} values and photocurrent confirmed that the PEC biosensor was successfully prepared.

3.4. Characterization of the PEC Biosensor. The photocurrent (Figure 4A) and EIS (Figure 4B) responses were used to reflect the capture ability of MDA-MB-231 by the TiO_2 NTs/Au/PEG/HAp electrodes. As shown in Figure 4A,B, there was little difference in the photocurrent and R_{et} values of the PEC biosensor after immersed in the MDA-MB-231 cell (500 cell/mL) solution (black curve), MDA-MB-231 cell (500 cell/mL) and BSA (500 ng/mL) mixed solution (red curve), and MDA-MB-231 cell (500 cell/mL), BSA (500 ng/mL), Hb (500 ng/mL), and IgG (500 ng/mL) mixed solution (blue curve), which shows that the prepared PEC biosensing interface has excellent selectivity to the MDA-MB-231 cell.

In Figure 4C, the output signal of the TiO_2 NTs/Au/PEG/HAp electrodes modified with the MDA-MB-231 cell (500 cell/mL) was evaluated, and the calculated relative standard deviation (RSD) of photocurrent response measured within 580 s was 0.17%. In addition, with regard to storage stability, the photocurrent of the TiO_2 NTs/Au/PEG/HAp/cell decreased by 3.56% after 1 week of storage.

Reproducibility reflects the reliability of the immunosensor, and the photocurrent RSD of five biosensors (a−e) with the modified cell (500 cell/mL) was 1.61% (Figure 4D). The final results proved that the TiO_2 NTs/Au/PEG/HAp electrodes modified with the cell also showed good stability and reproducibility.

https://doi.org/10.1021/acsabm.1c00215
ACS Appl. Bio Mater. 2021, 4, 4479−4485

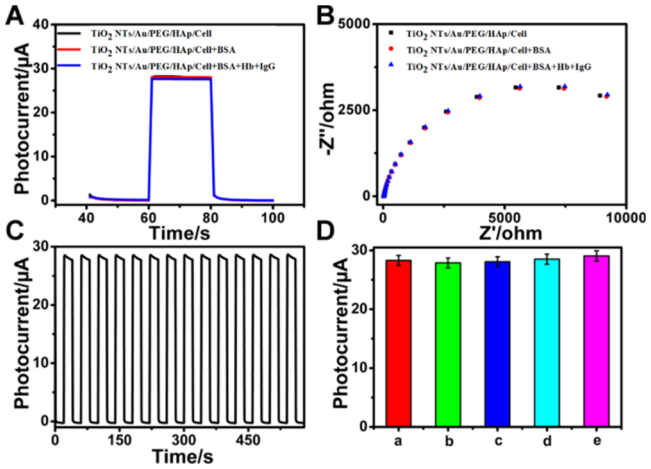

Figure 4. Photocurrent (A) and EIS (B) responses of the TiO_2 NTs/Au/PEG/HAp electrodes soaked in the MDA-MB-231 cell (500 cell/mL) solution, the mixed solution of MDA-MB-231 cell (500 cell/mL) and BSA (500 ng/mL), and the mixed solution of MDA-MB-231 cell (500 cell/mL), BSA (500 ng/mL), Hb (500 ng/mL), and IgG (500 ng/mL); photocurrent (C) of the TiO_2 NTs/Au/PEG/HAp electrode decorated with the cell (500 cell/mL) within 580 s; and (D) five biosensors (a−e) modified with the cell (500 cell/mL).

3.5. Quantitative Determination of MDA-MB-231.

MDA-MB-231 was quantitatively tested under optimal construction and detection conditions. As shown in Figure 5A, biosensors soaked in different concentrations of MDA-MB-231 suspension have different photocurrents, which indicate that the proposed PEC biosensor can be used for the quantitative determination of MDA-MB-231. When the MDA-MB-231 concentration range is 50 to 5.0×10^6 cell/mL, the photocurrent of the biosensor has a linear relationship with the logarithm of the MDA-MB-231 concentration (Figure 5B), and the linear equation is $y = -3.19 \lg c + 36.44$. The correlation coefficient and the limit of detection (LOD) were 0.9994 and 16 cells/mL, respectively.

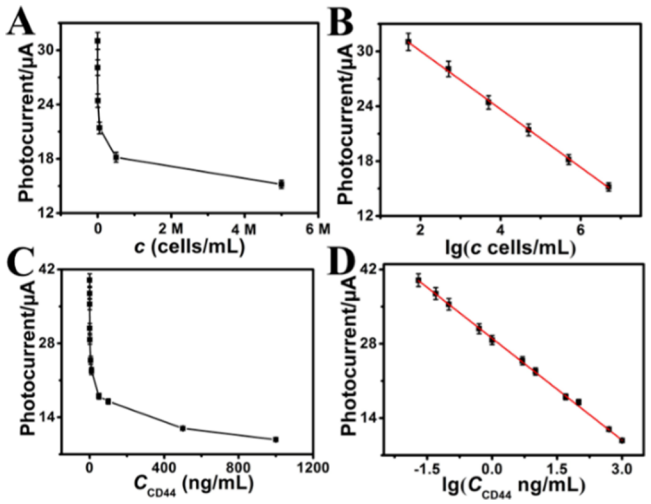

Figure 5. (A) Change of photocurrent with cell suspension concentration (50 to 5.0×10^6 cell/mL, M means million); (B) calibration curve of photocurrent and MDA-MB-231 cell concentration logarithm; (C) change of photocurrent with CD44 suspension concentration (0.020 to 1.0×10^3 ng/mL); and (D) calibration curve of photocurrent and CD44 concentration logarithm.

3.6. Evaluation of CD44 Expression.

Membrane-associated CD44 can be enzymatically hydrolyzed into a serum-soluble form.[40] Furthermore, the concentration of soluble CD44 in tumor patients is significantly higher than that in normal people.[41] In addition, in order to further demonstrate that the photocurrent change was indeed caused by HAP and CD44-positive recognition, we studied the PEC biosensor modified with soluble CD44. The experimental process is similar to that of the cell (details of the process can be found in the Supporting Information).

We quantified soluble CD44 with the suggested PEC biosensors. As shown in Figure 5C, the PEC biosensors soaked in CD44 solution with different concentrations have different photocurrents. Furthermore, like MDA-MB-231 cell suspensions, when the soluble CD44 solution concentration range is 0.020 to 1.0×10^3 ng/mL, the LOD is 0.015 ng/mL. In Figure 5D, the regression equation of the calibration curve is observed to be $y = -6.40 \lg c + 29.03$ ($R^2 = 0.9997$). Meanwhile, different concentrations of CD44 were added to the serum for measuring its recovery for testing the detection capability of the PEC biosensor for soluble CD44 in actual sample analysis. The average recoveries of the PEC biosensor were in the range of 98.01−103.82% (Table S3).

At the same time, the performance of the CD44-modified PEC biosensor was studied. Figure S5A,B shows that the TiO_2 NTs/Au/PEG/HAp electrode has almost the same photocurrent and R_{et} values after being immersed in the single CD44 (10 ng/mL) solution (black curve), CD44 (10 ng/mL) and BSA (500 ng/mL) mixed solution (red curve), and CD44 (10 ng/mL), BSA (500 ng/mL), Hb (500 ng/mL), and IgG (500 ng/mL) mixed solution (blue curve), which means that the fabricated biosensor has good selectivity to CD44. As shown in Figure S5C, for the output signal of the TiO_2 NTs/Au/PEG/HAp electrodes decorated with CD44 (10 ng/mL), the RSD of photocurrent response within 580 s was 1.03%. In addition, the photocurrent of TiO_2 NTs/Au/PEG/HAp/CD44 decreased by 4.89% after 1 week of storage. The photocurrent RSD of five biosensors decorated with CD44 was 0.93% (Figure S5D). The final results proved that the TiO_2 NTs/Au/PEG/HAp electrodes decorated with CD44 also showed good stability and reproducibility.

4. CONCLUSIONS

In conclusion, based on the interaction between the ligand and the protein receptor, a novel label-free PEC biosensor based on TiO_2 NTs was designed for detecting MDA-MB-231($CD44^+$). By depositing Au NPs on TiO_2 NTs, PEG with antifouling ability was introduced onto the electrode surface, which greatly improved the antifouling ability of the biosensor. At the same time, HA is functionalized by DA to obtain HAp containing catechol, which makes it easier to be modified onto the electrode. The results showed that the PEC biosensing interface can not only achieve the quantitative detection of tumor cells through membrane-associated CD44 but also realize the quantitative detection of soluble CD44. Furthermore, the proposed PEC biosensor shows good antifouling performance for tumor cells and soluble CD44 detection with a wide detection range. Because of its good performance, especially its excellent antifouling ability, the PEC biosensor has good prospects in clinical applications.

https://doi.org/10.1021/acsabm.1c00215
ACS Appl. Bio Mater. 2021, 4, 4479−4485

■ ASSOCIATED CONTENT

Supporting Information

The Supporting Information is available free of charge at https://pubs.acs.org/doi/10.1021/acsabm.1c00215.

Details of materials, reagents, and apparatus; structural formula of SH-PEG; antifouling tests; study on the selectivity, stability, and repeatability of PEC biosensors modified with soluble CD44; XPS and UV−vis spectra of the TiO_2 NTs electrode and the TiO_2 NTs/Au electrode; and real-sample analysis of soluble CD44 (PDF)

■ AUTHOR INFORMATION

Corresponding Authors

Hongmin Ma − *Key Laboratory of Interfacial Reaction & Sensing Analysis in Universities of Shandong, School of Chemistry and Chemical Engineering, University of Jinan, Jinan 250022, P. R. China;* orcid.org/0000-0002-7061-8944; Phone: (86) 531 82765969; Email: mahongmin2002@126.com

Qin Wei − *Key Laboratory of Interfacial Reaction & Sensing Analysis in Universities of Shandong, School of Chemistry and Chemical Engineering, University of Jinan, Jinan 250022, P. R. China;* orcid.org/0000-0002-3034-8046; Phone: (86) 531 82760510; Email: sdjndxwq@163.com

Authors

Ning Gao − *Key Laboratory of Interfacial Reaction & Sensing Analysis in Universities of Shandong, School of Chemistry and Chemical Engineering, University of Jinan, Jinan 250022, P. R. China*

Bobo Fan − *Key Laboratory of Interfacial Reaction & Sensing Analysis in Universities of Shandong, School of Chemistry and Chemical Engineering, University of Jinan, Jinan 250022, P. R. China*

Li Li − *Key Laboratory of Interfacial Reaction & Sensing Analysis in Universities of Shandong, School of Chemistry and Chemical Engineering, University of Jinan, Jinan 250022, P. R. China*

Xiaojun Sun − *Key Laboratory of Interfacial Reaction & Sensing Analysis in Universities of Shandong, School of Chemistry and Chemical Engineering, University of Jinan, Jinan 250022, P. R. China*

Xueying Wang − *Key Laboratory of Interfacial Reaction & Sensing Analysis in Universities of Shandong, School of Chemistry and Chemical Engineering, University of Jinan, Jinan 250022, P. R. China*

Huangxian Ju − *Key Laboratory of Interfacial Reaction & Sensing Analysis in Universities of Shandong, School of Chemistry and Chemical Engineering, University of Jinan, Jinan 250022, P. R. China;* orcid.org/0000-0002-6741-5302

Complete contact information is available at: https://pubs.acs.org/10.1021/acsabm.1c00215

Author Contributions

[†]N.G. and B.F. contributed equally to this work.

Notes

The authors declare no competing financial interest.

■ ACKNOWLEDGMENTS

This study was financially supported by the Shandong Provincial Natural Science Foundation (ZR2020YQ13), A Project of Shandong Province Higher Educational Youth Innovation Science and Technology Program (2020KJC008), and the Jinan Scientific Research Leader Workshop Project (2018GXRC024). Institute for Smart Materials & Engineering, University of Jinan is acknowledged for the characterization of new compounds.

■ REFERENCES

(1) Orian-Rousseau, V. CD44, A therapeutic target for metastasising tumours. *Eur. J. Canc.* **2010**, *46*, 1271−1277.

(2) Higashikawa, K.; Yokozaki, H.; Ue, T.; Taniyama, K.; Ishikawa, T.; Tarin, D.; Tahara, E. Evaluation of CD44 transcription variants in human digestive tract carcinomas and normal tissues. *Int. J. Cancer* **1996**, *66*, 11−17.

(3) Ikegami-Kawai, M.; Takahashi, T. Microanalysis of hyaluronan oligosaccharides by polyacrylamide gel electrophoresis and its application to assay of hyaluronidase activity. *Anal. Biochem.* **2002**, *311*, 157−165.

(4) Toole, B. P. Hyaluronan: from extracellular glue to pericellular cue. *Nat. Rev. Cancer* **2004**, *4*, 528−539.

(5) Huang, Y.; Yao, X.; Zhang, R.; Ouyang, L.; Jiang, R.; Liu, X.; Song, C.; Zhang, G.; Fan, Q.; Wang, L.; Huang, W. Cationic conjugated polymer/fluoresceinamine-hyaluronan complex for sensitive fluorescence detection of CD44 and tumor-targeted cell imaging. *ACS Appl. Mater. Interfaces* **2014**, *6*, 19144−19153.

(6) Ju, Y.; Cui, J.; Sun, H.; Müllner, M.; Dai, Y.; Guo, J.; Bertleff-Zieschang, N.; Suma, T.; Richardson, J. J.; Caruso, F. Engineered metal-phenolic capsules show tunable targeted delivery to cancer cells. *Biomacromolecules* **2016**, *17*, 2268−2276.

(7) Spadea, A.; Rios de la Rosa, J. M.; Tirella, A.; Ashford, M. B.; Williams, K. J.; Stratford, I. J.; Tirelli, N.; Mehibel, M. Evaluating the efficiency of hyaluronic acid for tumor targeting via CD44. *Mol. Pharm.* **2019**, *16*, 2481−2493.

(8) Phillips, J. A.; Xu, Y.; Xia, Z.; Fan, Z. H.; Tan, W. Enrichment of cancer cells using aptamers immobilized on a microfluidic channel. *Anal. Chem.* **2009**, *81*, 1033−1039.

(9) Liu, M.; Xu, Y.; Huang, C.; Jia, T.; Zhang, X.; Yang, D.; Jia, N. Hyaluronic acid-grafted three-dimensional MWCNT array as biosensing interface for chronocoulometric detection and fluorometric imaging of CD44-overexpressing cancer cells. *Microchim. Acta* **2018**, *185*, 338.

(10) Pantel, K.; Brakenhoff, R. H.; Brandt, B. Detection, clinical relevance and specific biological properties of disseminating tumour cells. *Nat. Rev. Cancer* **2008**, *8*, 329−340.

(11) Wang, X.; Wang, X.; Cheng, S.; Ye, M.; Zhang, C.; Xian, Y. Near-Infrared Light-Switched MoS_2 Nanoflakes@Gelatin Bioplatform for Capture, Detection, and Nondestructive Release of Circulating Tumor Cells. *Anal. Chem.* **2020**, *92*, 3111−3117.

(12) Wang, Z.; Li, J.; Tu, W.; Wang, H.; Wang, Z.; Dai, Z. Formation of a Photoelectrochemical Z-Scheme Structure with Inorganic/Organic Hybrid Materials for Evaluation of Receptor Protein Expression on the Membrane of Cancer Cells. *ACS Appl. Mater. Interfaces* **2020**, *12*, 26905−26913.

(13) Zhu, L.; Wei, T.; Yu, R.; Tu, W.; Dai, Z. A versatile switchable dual-modal colorimetric and photoelectrochemical biosensing strategy via light-controlled sway of a signal-output transverter. *Chem. Commun.* **2021**, *57*, 3223.

(14) Li, J.; Lin, X.; Zhang, Z.; Tu, W.; Dai, Z. Red light-driven photoelectrochemical biosensing for ultrasensitive and scatheless assay of tumor cells based on hypotoxic $AgInS_2$ nanoparticles. *Biosens. Bioelectron.* **2019**, *126*, 332−338.

(15) Cheng, W.; Pan, J.; Yang, J.; Zheng, Z.; Lu, F.; Chen, Y.; Gao, W. A photoelectrochemical aptasensor for thrombin based on the use

of carbon quantum dot-sensitized TiO_2 and visible-light photoelectrochemical activity. *Microchim. Acta* **2018**, *185*, 263.
(16) Ma, X.; Wang, X.; Yu, C.; Song, Y.; Liang, J.; Min, Q.; Zhang, F. Effects of primary nanobuilding blocks on the photocatalytic performance of TiO_2 hierarchical hollow microspheres. *J. Alloys Compd.* **2019**, *773*, 352−360.
(17) Naldoni, A.; Altomare, M.; Zoppellaro, G.; Liu, N.; Kment, Š.; Zbořil, R.; Schmuki, P. Photocatalysis with reduced TiO_2: from black TiO_2 to cocatalyst-free hydrogen production. *ACS Catal.* **2019**, *9*, 345−364.
(18) Kim, J. K.; Chai, S. U.; Ji, Y.; Levy-Wendt, B.; Kim, S. H.; Yi, Y.; Heinz, T. F.; Nørskov, J. K.; Park, J. H.; Zheng, X. Resolving hysteresis in perovskite solar cells with rapid flame-processed cobalt-doped TiO_2. *Adv. Energy Mater.* **2018**, *8*, 1801717.
(19) Li, Y.; Lu, Q.; Liu, H.; Wang, J.; Zhang, P.; Liang, H.; Jiang, L.; Wang, S. Antibody-Modified reduced graphene oxide films with extreme sensitivity to circulating tumor cells. *Adv. Mater.* **2016**, *27*, 6848−6854.
(20) Wang, S.; Liu, K.; Liu, J.; Yu, Z. T.-F.; Xu, X.; Zhao, L.; Lee, T.; Lee, E. K.; Reiss, J.; Lee, Y.-K.; Chung, L. W. K.; Huang, J.; Rettig, M.; Seligson, D.; Duraiswamy, K. N.; Shen, C. K.-F.; Tseng, H.-R. Titelbild: highly efficient capture of circulating tumor cells by using nanostructured silicon substrates with integrated chaotic micromixers. *Angew. Chem. Int. Ed.* **2011**, *123*, 2909.
(21) Fan, B.; Fan, Q.; Cui, M.; Wu, T.; Wang, J.; Ma, H.; Wei, Q. Photoelectrochemical biosensor for sensitive detection of soluble CD44 based on the facile construction of a polyethylene glycol/hyaluronic acid hybrid antifouling interface. *ACS Appl. Mater. Interfaces* **2019**, *11*, 24764−24770.
(22) Hui, N.; Sun, X.; Niu, S.; Luo, X. PEG-ylated polyaniline nanofibers: antifouling and conducting biomaterial for electrochemical DNA sensing. *ACS Appl. Mater. Interfaces* **2017**, *9*, 2914−2923.
(23) Chen, L.; Lv, S.; Gao, Z.; Chen, C. Voltammetric immunoassay for the carcinoembryonic antigen by using a glassy carbon electrode modified with poly(3,4-ethylenedioxythiophene) doped with tannic acid and grafted with poly(ethylene glycol). *Microchim. Acta* **2017**, *184*, 4705−4712.
(24) Kim, J. H.; Lee, M.; Park, C. B. Polydopamine as a biomimetic electron gate for artificial photosynthesis. *Angew. Chem.* **2014**, *53*, 6364−6368.
(25) Huang, H.; Bai, W.; Dong, C.; Guo, R.; Liu, Z. An ultrasensitive electrochemical DNA biosensor based on graphene/Au nanorod/polythionine for human papillomavirus DNA detection. *Biosens. Bioelectron.* **2015**, *68*, 442−446.
(26) Fang, X.; Liu, J.; Wang, J.; Zhao, H.; Ren, H.; Li, Z. Dual signal amplification strategy of Au nanopaticles/ZnO nanorods hybridized reduced graphene nanosheet and multienzyme functionalized Au@ZnO composites for ultrasensitive electrochemical detection of tumor biomarker. *Biosens. Bioelectron.* **2017**, *97*, 218−225.
(27) Ye, Q.; Zhou, F.; Liu, W. Bioinspired catecholic chemistry for surface modification. *Chem. Soc. Rev.* **2011**, *40*, 4244−4258.
(28) Dreyer, D. R.; Miller, D. J.; Freeman, B. D.; Paul, D. R.; Bielawski, C. W. Elucidating the Structure of Poly(dopamine). *Langmuir* **2012**, *28*, 6428−6435.
(29) Anderson, T. H.; Yu, J.; Estrada, A.; Hammer, M. U.; Waite, J. H.; Israelachvili, J. N. The contribution of DOPA to substrate-peptide adhesion and internal cohesion of mussel-inspired synthetic peptide films. *Adv. Funct. Mater.* **2010**, *20*, 4196−4205.
(30) Vatankhah-Varnosfaderani, M.; Hu, X.; Li, Q.; Adelnia, H.; Ina, M.; Sheiko, S. S. Universal coatings based on zwitterionic-dopamine copolymer microgels. *ACS Appl. Mater. Interfaces* **2018**, *10*, 20869−20875.
(31) Zhao, F.-Y.; Ji, Y.-L.; Weng, X.-D.; Mi, Y.-F.; Ye, C.-C.; An, Q.-F.; Gao, C.-J. High-Flux positively charged nanocomposite nanofiltration membranes filled with poly(dopamine) modified multiwall marbon nanotubes. *ACS Appl. Mater. Interfaces* **2016**, *8*, 6693−6700.
(32) Shin, J.; Lee, J. S.; Lee, C.; Park, H.-J.; Yang, K.; Jin, Y.; Ryu, J. H.; Hong, K. S.; Moon, S.-H.; Chung, H.-M.; Yang, H. S.; Um, S. H.; Oh, J.-W.; Kim, D.-I.; Lee, H.; Cho, S.-W. Tissue adhesive catechol-modified hyaluronic acid hydrogel for effective, minimally invasive cell therapy. *Adv. Funct. Mater.* **2015**, *25*, 3814−3824.
(33) Burdick, J. A.; Prestwich, G. D. Hyaluronic Acid Hydrogels for Biomedical Applications. *Adv. Mater.* **2011**, *23*, H41−H56.
(34) Highley, C. B.; Prestwich, G. D.; Burdick, J. A. Recent Advances in Hyaluronic Acid Hydrogels for Biomedical Applications. *Curr. Opin. Biotechnol.* **2016**, *40*, 35−40.
(35) Hong, S.; Yang, K.; Kang, B.; Lee, C.; Song, I. T.; Byun, E.; Park, K. I.; Cho, S.-W.; Lee, H. Hyaluronic acid catechol: a biopolymer exhibiting a pH-dependent adhesive or cohesive property for human neural stem cell engineering. *Adv. Funct. Mater.* **2013**, *23*, 1774−1780.
(36) Liu, X.-P.; Chen, J.-S.; Mao, C.-j.; Niu, H.-L.; Song, J.-M.; Jin, B.-K. Enhanced photoelectrochemical DNA sensor based on TiO_2/Au hybrid structure. *Biosens. Bioelectron.* **2018**, *116*, 23−29.
(37) Xue, J.; Shen, Q.; Liang, W.; Liu, X.; Yang, F. Photosensitization of TiO_2 nanotubearrays with CdSe nanoparticles and their photoelectrochemical performanceunder visible light. *Electrochim. Acta* **2013**, *97*, 10−16.
(38) Maicu, M.; Hidalgo, M. C.; Colón, G.; Navío, J. A. Comparative study of thephotodeposition of Pt, Au and Pd on presulphated TiO_2 for the photocatalyticdecomposition of phenol. *J. Photochem. Photobiol., A* **2011**, *217*, 275−283.
(39) Lickleder, M.; Mohammadi, R.; Nguyen, N. T.; Park, H.; Hejazi, S.; Halik, M.; Vogel, N.; Altomare, M.; Schmuki, P. Dewetted Au Nanoparticles on TiO_2 Surfaces: Evidence of a Size-Independent Plasmonic Photoelectrochemical Response. *J. Phys. Chem. C* **2019**, *123*, 16934−16942.
(40) Masson, D.; Denis, M. G.; Denis, M.; Blanchard, D.; Loirat, M. J.; Cassagnau, E.; Lustenberger, P. Soluble CD44: quantification and molecular repartition in plasma of patients with colorectal cancer. *Br. J. Cancer* **1999**, *80*, 1995−2000.
(41) Franzmann, E. J.; Reategui, E. P.; Pedroso, F.; Pernas, F. G.; Karakullukcu, B. M.; Carraway, K. L.; Hamilton, K.; Singal, R.; Goodwin, W. J. Soluble CD44 is a potential marker for the early detection of head and neck cancer. *Cancer Epidemiol., Biomarkers Prev.* **2007**, *16*, 1348−1355.

https://doi.org/10.1021/acsabm.1c00215
ACS Appl. Bio Mater. 2021, 4, 4479−4485